Desiccant wheels effectiveness parameters: Correlations based on experimental data

Stefano De Antonellis*, Manuel Intini, Cesare Maria Joppolo

Dipartimento di Energia, Politecnico di Milano, Via Lambruschini, 4, 20156 Milan, Italy

Received 9 January 2015
Received in revised form 4 June 2015
Accepted 14 June 2015
Available online 20 June 2015

1. Introduction

At present interest in desiccant evaporative cooling (DEC) cycles is strongly increasing due to the possibility of realizing low envi-ronmental impact and high energy efficiency HVAC systems driven by low temperature heat and renewable energy [1,2]. This emerg-ing technology can be properly used in applications for air cooling and dehumidification [3–7] or in the industrial field for product drying processes [8–10]. In these systems the air dehumidification treatment is typically reached through a desiccant wheel, which is obtained rolling up sheets of a supporting material coated with an adsorbent substance, in order to get a large number of paral-lel channels. Two air streams in counter current arrangement flow through the device: the process air, which is dehumidified and heated, and the regeneration air, which removes water from the adsorbent material [11].

It is well-known that the desiccant wheel is a crucial component in DEC systems. At present research works are mainly focused on component models and experimental tests [12–16], new device or system arrangements [17,18], new sorption materials [19] and systems optimization [20–22]. Desiccant wheel performance is strongly influenced by operating conditions, namely process and regeneration air temperature, humidity and face velocity and revolution speed. In simulations of energy systems based on DEC technology, prediction of desiccant wheel performance is of critical importance in order to get proper and correct results. The use of detailed component models based on heat and mass transfer equations is not suggested due to the high computational load and, therefore, simplified methods are recommended.

Several works deal with the evaluation of simplified approaches to determine desiccant wheel performance. Beccali et al. [23,24] proposed experimental correlations based on manufacturer data for balanced and unbalanced air flows. These correlations have been widely used in literature but they are not related to a specific air face velocity and revolution speed.

Some works focus on the analysis of performance through a pair of effectiveness parameters. Panaras et al. [25] investigated experimentally the constant combined potential approach based on the formulation proposed by Jurinak [26]. In that work a commercial silica gel desiccant wheel has been tested at constant revolution speed and balanced air flows. It is shown that the effectiveness factors remain constant over a sufficiently wide range of operat-ing conditions. Ruivo and Angrisani [27] put in evidence that this constant effectiveness approach is not still valid in case of variable revolution speed and unbalanced air flows. Moreover the combined potential approach is widely considered rather complex in order to be effectively adopted. In several works the desiccant wheel dehumidification capacity is evaluated through humidity ratio and temperature effectiveness indices [28–30]. Ali Mandegari and Pahlavanzadeh [30] proposed an effectiveness parameter based on enthalpy difference and analyzed its trend referring to experimental data. Ruivo et al. [31] introduced three new

* Corresponding author.
E-mail address: stefano.deantonellis@polimi.it (S. De Antonellis).

Nomenclature

a	channel height (mm)
b	channel base (mm)
cp	specific heat (kJ kg^{-1} K^{-1})
$c_{1,2,\dots 12}$	η_ϕ correlation parameters
$k_{1,2,\dots 11}$	η_h correlation parameters
h	enthalpy (kJ kg^{-1})
Le	Lewis number
m	mass flow rate (kg s^{-1})
N	revolution speed (rev h^{-1})
Nu	Nusselt number
N_{test}	number of experimental tests
p	pressure (Pa)
p_{tot}	atmospheric pressure (Pa)
$RMSE$	root mean square error (°C or kg$_v$ kg$_{da}^{-1}$)
Sh	Sherwood number
T	temperature (°C)
u	uncertainty
v	face velocity (m s^{-1})
V	air flow rate (m^3 s^{-1})
$x_{1,2}$	Δp correlation parameters
X	humidity ratio (kg$_v$ kg$_{da}^{-1}$)

Greek Symbols

α	η_ϕ correlation terms
β	η_h correlation terms
ΔP	pressure drop (Pa)
ΔT	temperature difference (°C)
ΔX	humidity ratio difference (kg$_v$ kg$_{da}^{-1}$)
η	effectiveness
ϕ	relative humidity
λ	water latent heat of vaporization (kJ kg^{-1})
ρ	density (kg m^{-3})
μ	dynamic viscosity (kg m^{-1} s^{-1})
σ	wheel porosity

Subscripts

a	air
ads	desiccant wheel sorption material
da	dry air
EXP	experimental
in	inlet
N	revolution speed
out	outlet
opt	optimal
pro	process air
reg	regeneration air
T	temperature
v	water vapour
$vpro$	process air face velocity
$vreg$	regeneration air face velocity
$vsat$	saturated vapour
X	humidity ratio

effectiveness indices that are calculated respectively through the variation of process air relative humidity, adsorbed water content and air enthalpy. In this work the use of this effectiveness pair is investigated at constant and balanced air flows. This approach has been analyzed in further works [32–34] and detailed interpolation methods are evaluated in order to take into account the effect of inlet air states, airflow rates and the revolution speed. Finally Ruivo et al. [35] compared several interpolation methods to predict process air outlet conditions at low regeneration

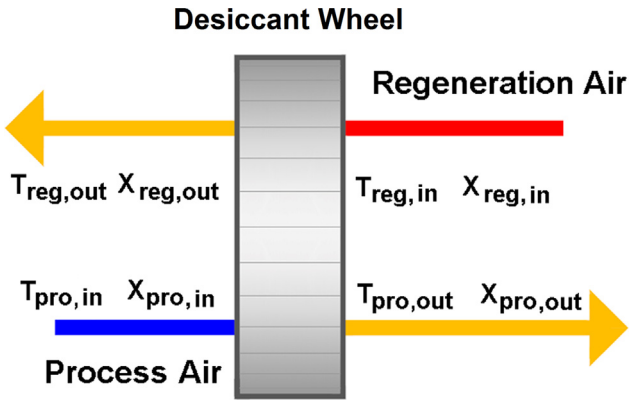

Fig. 1. Desiccant wheel scheme.

temperature and analyzed the influence of rotational speed on effectiveness parameters [36].

According to current state of the art, the effectiveness parameters based on the psychrometric variables ϕ and h are particularly suitable to predict the desiccant wheel performance. Anyway in the available studies the effectiveness correlations are based on manufacturer data or on a limited number of experimental tests and they do not take into account the variation of all inlet conditions. In addition pressure drop data is not provided, although such information is particularly important in the study of DEC systems. Therefore, the aim of this work is:

- To preliminary investigate the influence of operating conditions on the effectiveness parameters based on the psychometric variables ϕ and h.
- To provide practical effectiveness correlations based on experimental data that take into account a wide variation of all operating conditions.
- To provide a correlation to evaluate air pressure drop across the wheel.

The proposed correlations to predict the outlet process air conditions and pressure drop are a useful tool that can be effectively used in energy systems simulation and that can be integrated in commercial software, such as TRNSYS and Energy Plus.

2. Enthalpy and relative humidity effectiveness parameters

2.1. Parameters definition

Referring to Fig. 1, the effectiveness pair proposed by Ruivo et al.[31] that is used in this work is defined in the following way:

$$\eta_\phi = \frac{\phi_{pro,in} - \phi_{pro,out}}{\phi_{pro,in} - \phi_{reg,in}} \tag{1}$$

$$\eta_h = \frac{h_{pro,out} - h_{pro,in}}{h_{reg,in} - h_{pro,in}} \tag{2}$$

If inlet air conditions of both air streams and the effectiveness parameters are known, the enthalpy and relative humidity of outlet process air stream are obtained. Therefore, temperature, humidity ratio and water vapour saturation pressure can be easily calculated through the following equations:

$$X_{pro,out} = 0.622 \frac{\phi_{pro,out}}{(p_{tot}/p_{pro,out,vsat}) - \phi_{pro,out}} \tag{3}$$

$$T_{pro,out} = \frac{h_{pro,out} - \lambda X_{pro,out}}{cp_{da} + X_{pro,out} cp_v} \tag{4}$$

$$p_{pro,out,vsat} = e^{23.196-\frac{3816.44}{T_{pro,out}+273.15-46.13}} \quad (5)$$

where p_{tot} has been assumed constant and equal to 101325 Pa and the latent heat of water vaporization is λ = 2501 kJ kg^{-1}.

2.2. Preliminary theoretical considerations

As described in Section 1, the effectiveness parameters η_ϕ and η_h strongly depend on air inlet states and on revolution speed [32,33]. In order to evaluate appropriate correlations, preliminary considerations are provided. Referring to Eqs. (1) and (2), it is discussed how the variation of every inlet air condition, keeping constant the others, affects the effectiveness parameters η_ϕ and η_h. It is possible to state that:

- An increase in $T_{pro,in}$ leads to a decrease in $\phi_{pro,in}$ and to an increase in $h_{pro,in}$. The dehumidification capacity decreases and, therefore, an increase in $X_{pro,out}$ and $h_{pro,out}$ is shown [11]. As a consequence both denominators of Eqs. (1) and (2) decrease and it is not pos-sible to predict the behaviour of the two numerators exactly. Ali Mandegari and Pahlavanzadeh [30] evaluated experimentally the trend of η_h as a function of $T_{pro,in}$ and found out that there is an optimal value of η_h and that the effectiveness parameter does not strictly increase or decrease with $T_{pro,in}$. It is put in evidence in that work the effectiveness parameter is defined in a slightly different form compared to the one reported in Eq. (2).
- The higher $X_{pro,in}$, the higher $\phi_{pro,in}$, $h_{pro,in}$, $X_{pro,out}$, $T_{pro,out}$ (due to the higher amount of adsorbed vapour) and $h_{pro,out}$. Depending on the actual variation of $h_{pro,in}$, $\phi_{pro,in}$, $\phi_{pro,out}$ and $h_{pro,out}$, it is expected that η_h and η_ϕ can increase or decrease.
- An increase in $v_{pro,in}$ leads to a reduction in $T_{pro,out}$ and to an increase in $X_{pro,out}$ and $\phi_{pro,out}$ [37]. A higher airflow rate cools down the desiccant matrix faster and speed up the dehumidification process. However, higher flow rates lead to smaller drop in process flow humidity ratio and, in turn, to a smaller rise in process flow temperature. As a consequence, if N is equal or higher than the optimal revolution speed, it is expected $h_{pro,out}$ decreases, leading to a lower η_h. Similarly $\phi_{pro,out}$ increases and consequently η_ϕ decreases.
- In typical working conditions of HVAC systems, if $T_{reg,in}$ increases the dehumidification process becomes more effective: the outlet process air reaches a higher temperature and a lower relative humidity while the inlet regeneration air flow slightly decreases its relative humidity. In most cases numerator of Eq. (1) increases, denominator slightly increases (in particular at high regeneration temperature) and therefore an increase in η_ϕ is expected. In addition the higher $T_{reg,in}$, the higher $h_{reg,in}$: depending on the actual variation of $h_{pro,out}$, η_h could increase or decrease. Ali Mandegari and Pahlavanzadeh [30] highlighted that η_h mainly increases with $T_{reg,in}$, showing also a local optimum point. Both expected trends of η_ϕ and η_h are confirmed also by Ruivo et al. [31], who calculated the effectiveness pair from experimental data of Kuma et al. [38]. They show that an increase in $T_{reg,in}$ generally leads to a slight increase in η_ϕ and to an increase or decrease in η_h.
- When $X_{reg,in}$ increases, $h_{reg,in}$ and $\phi_{reg,in}$ also increase and the dehumidification process becomes less effective. Therefore $\phi_{pro,out}$ is higher than the reference condition: both numerator and denominator of Eq. (1) decrease and therefore η_ϕ could either increase or decrease. Due to the lower dehumidification performance, less heat of adsorption is released to the process air stream but at the same time more heat is transferred through the wheel matrix which is kept slightly warmer in the regeneration period. Also in this case it is not possible to predict $h_{pro,out}$ and therefore the variation of η_h. Ruivo et al. [31] calculated the effectiveness parameters for different values of X_{in} (with balanced air flows and $X_{pro,in}$ equal to $X_{reg,in}$). They show that an increase in X_{in} leads to a decrease in η_h and to a slight increase or decrease in η_ϕ.
- An increase in $v_{reg,in}$ leads to an enhancement of the dehumidification process [37]. Therefore $\phi_{pro,out}$ decreases and an increase in η_ϕ is shown. On the other side $h_{pro,out}$ and, therefore, η_h may either increase or decrease.
- According to previous research works [30,31,36], the higher the revolution speed, the higher the heat transferred [14,15] and η_h. In fact, due to the typical low revolution speed of desiccant wheels, an increase in N leads to an increase in the heat transferred and, therefore, in the outlet process air temperature and enthalpy. At low revolution speed, the wheel matrix temperature becomes close to the air stream one and, therefore, heat transfer decreases. Finally, according to the analysis provided by Enteria et al. [15], there is an optimal revolution speed below which η_ϕ rapidly drops down (not optimized working conditions) and above which η_ϕ slightly decrease. Similarly Ruivo et al. [31,36] show that an increase in N initially leads to a significant increase in η_ϕ and gradually, when the optimal revolution speed is approached, to an almost constant effectiveness value.

Based on the aforementioned theoretical analysis, it turns out that all boundary conditions have effects on both adopted effectiveness parameters. In particular it is shown that:

- An increase in $v_{pro,in}$ leads to a decrease in η_ϕ and η_h.
- An increase in $T_{reg,in}$, $v_{reg,in}$ and N leads to an increase in η_ϕ.
- η_ϕ is slightly dependent on N.

It is expected that a good correlation is able to properly predict the aforementioned trends. About the effects of the variation of the other boundary conditions on η_ϕ and η_h, it is not possible to assess a general rule.

3. Experimental methodology

3.1. Experimental setup

In order to analyze desiccant wheels performance in different working conditions, a test facility has been properly designed. Experimental results are used to determine adequate correlations to predict the pair of effectiveness given in Eqs. (1) and (2) and to evaluate air pressure drop across the component.

The test rig is shown in Fig. 2 and it is designed to provide process and regeneration air streams at accurate controlled conditions of temperature, humidity and mass flow rate. The two air streams flows across the desiccant wheel in counter-current arrangement. Temperature and humidity are properly controlled through heating coils, cooling coils and evaporative coolers. In the regeneration air stream unit an additional electrical heater is installed in order to adjust the flow temperature up to 100 °C (in recirculation mode).

The desiccant wheel casing is divided in four equal partitions and each stream enters and leaves the casing through two of them. Temperature of each air stream is measured at the inlet section (in one point) and outlet section (in two points) of the casing through RTD PT100 sensors.

Humidity ratio is calculated from the measured values of temperature and relative humidity. For process inlet air stream, the temperature sensor is coupled with a relative humidity capacitive sensor. In all other cases, coupled temperature and relative humidity sensors have been arranged as follows (Fig. 2):

- In the regeneration air handling unit before the electric heater, in order to avoid measurement at very low relative humidity and, therefore, to reduce uncertainty of $X_{reg,in}$.

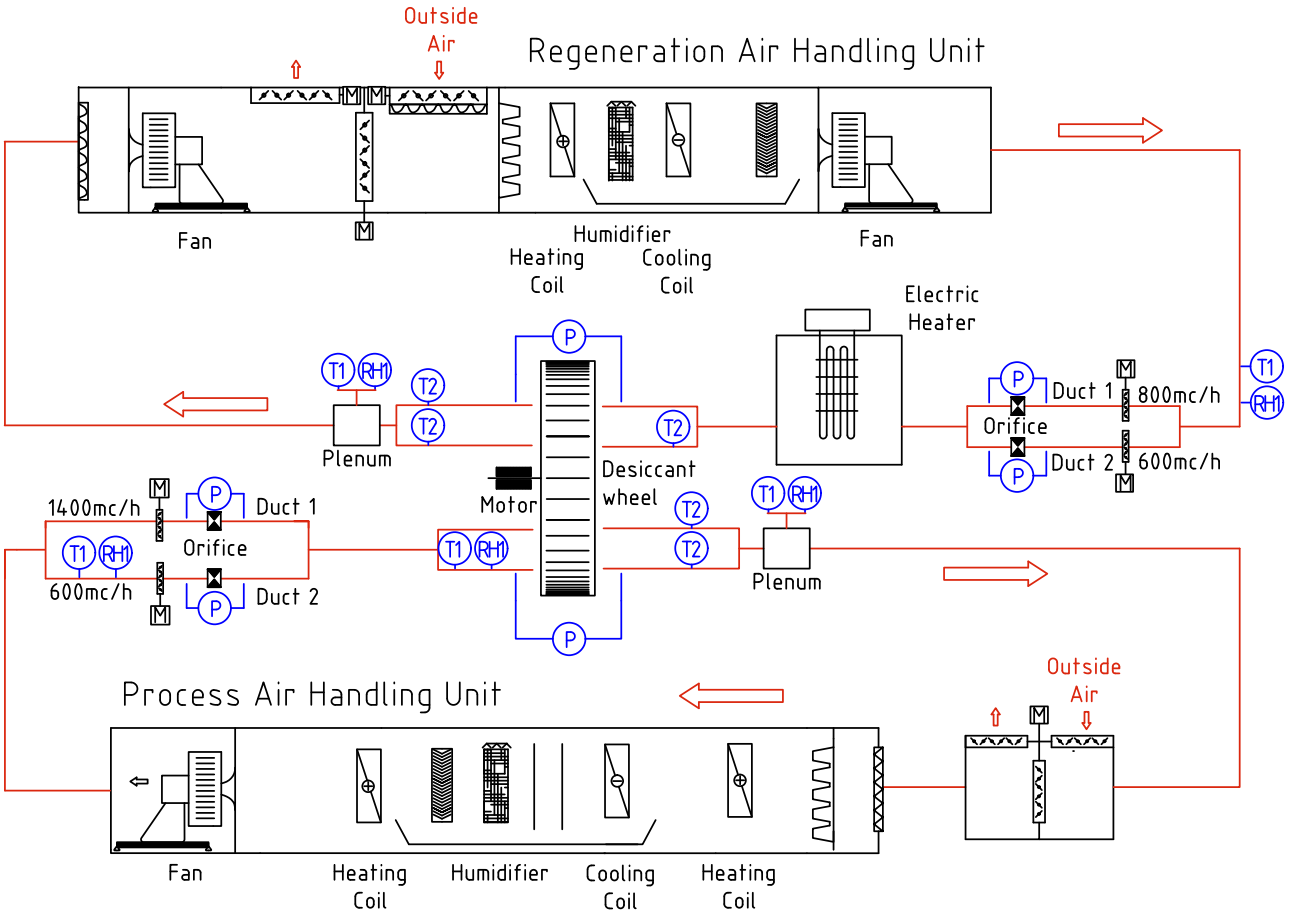

Fig. 2. Layout of the experimental setup.

- In the plenum where the two outlet regeneration air streams achieve a proper level of mixing. More precisely a sampling of regeneration outlet flow is extracted through a non-insulated duct that acts as an air cooler. Sensors are installed in the cooling duct, so that relative humidity measurement is more accurate because of the lower air temperature and higher relative humidity. Care must be taken not to incur in water vapour condensation in the sampling duct, which may detrimentally affect the measurement.
- In the plenum where the two outlet process air streams are mixed, as already described for the regeneration air flow.

Volumetric flow rates are controlled by variable speed fans and each one is measured through two orifice plates installed in two different parallel ducts. The maximum process air flow rate is 2000 $m^3\ h^{-1}$ and the maximum regeneration air flow rate is 1400 $m^3\ h^{-1}$. Orifice plates and ducts apparatus are constructed according to technical standards [39,40]. Pressure drop across the orifices and across the desiccant wheel is measured by piezoelec-tric transmitters. Main data of calibrated sensors are summarized in Table 1.

Finally desiccant wheel revolution speed can be manually controlled in the range between 5 and 30 rev h^{-1} and all sensors and actuators are connected to a NI Compact Rio system and controlled with LabVIEW software.

3.2. Experimental procedure

For each test experimental data are collected in steady state conditions and in each session at least 300 samples of every physical quantity are logged with a frequency of 1 Hz.

Table 1
Sensors main data.

Abbreviation	Type of sensor	Accuracy[a]
T1[b]	PT 100 Class A	±0.2 °C
T2	PT 100 Class A	±0.2 °C
RH1[b]	Capacitive	±1% (between 0 and 90%)
P	Piezoelectric	±0.5% of reading ± 1 Pa

[a] At $T = 20$ °C.
[b] Temperature and relative humidity probe.

The humidity ratio is calculated from the measured value of temperature and relative humidity with Eqs. (3)–(5).

The level of uncertainty of temperature and humidity ratio is estimated in accordance with the work by Moffat [41]. The experimental uncertainty u_{xi} of each direct monitored variable x_i, such as T_a, ϕ_a and p, is:

$$u_{x_i} = \pm\sqrt{u_{x_{i,inst}}^2 + (t_{95}\sigma_{\bar{x}_i})^2} \tag{6}$$

where $u_{xi,inst}$ is the instrument uncertainty of the generic measured parameter, t_{95} is the student test multiplier at 95% confidence and $\sigma_{\bar{x}_i}$ is the standard deviation of the mean.

The generic combined uncertainty u_ε of calculated quantities ε, such as X_a, ΔX_{pro} and ΔT_{pro} is calculated as:

$$u_\varepsilon = \sqrt{\sum_i \left(\frac{\partial \varepsilon}{\partial x_i} u_{x_i,inst}\right)^2 + t_{95}^2 \sum_i \left(\frac{\partial \varepsilon}{\partial x_i}\sigma_{\bar{x}_i}\right)^2} \tag{7}$$

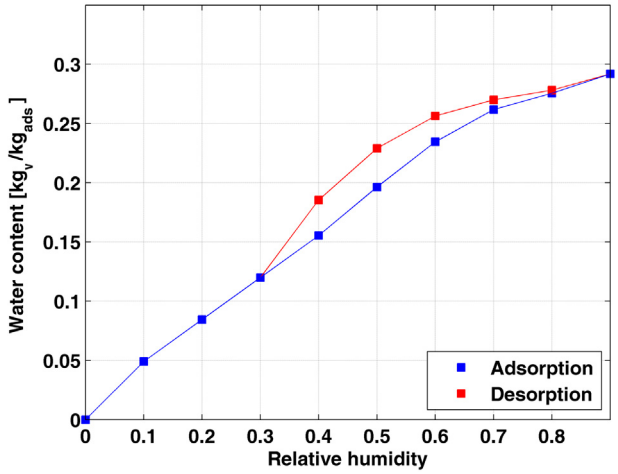

Fig. 3. Adsorption and desorption isotherm (T = 50 °C) of a sample of the desiccant wheel material.

3.3. Experimental tests

The tested desiccant wheel is a commercial device available on the market with outer diameter of 60 cm and an axial length of 20 cm. Channels have a sinusoidal cross sectional area with height a = 1.8 mm, base b = 3.55 mm and aspect ratio a/b = 0.51. Based on the channel aspect ratio value, in fully developed laminar flow condition the Nusselt number (at constant wall temperature) is $Nu \approx 2.1$, the Sherwood number is $Sh = Nu \approx 2.1$ (assuming $Le = 1$) and the friction factor is $f \approx 11/Re$ [42]. In addition the wheel poros-ity (free channel area to face area ratio) σ is equal to 0.76.

The wheel is made of synthesized metal silicate on inorganic fibre substrate (net organics less than 2%). A sample of the desiccant wheel (support and sorption material) has been collected on order to measure the adsorption isotherm with a dynamic vapour sorption analyzer. As reported in Fig. 3, the adsorption isotherm shows a Type IV trend, according to the IUPAC classification [43]. The component is split in two equal sections, each one crossed by the process and the regeneration air flow respectively. A purge sector is not installed.

On the whole 56 tests have been performed in steady states by varying $T_{pro,in}$, $X_{pro,in}$, $v_{pro,in}$, $T_{reg,in}$, $X_{reg,in}$, $v_{reg,in}$ and N in a wide range of operating conditions, as summarized in Table 2. Detailed inlet conditions and process air outlet states of each test are reported in Appendix A. In the investigated desiccant wheel ΔX_{pro} is around 4 g kg^{-1} when inlet process and regeneration air temperature, face velocity and inlet humidity ratio are respectively around 30 °C, 60 °C, 2 m s^{-1} and 12 g kg^{-1} (summer conditions). The achieved dehumidification capacity is almost comparable with one of the available desiccant wheels working in similar operating conditions [14,15,38] with different physical and geometric specifications.

In addition, a specific set of tests has been performed to evaluate pressure drop across the desiccant wheel as a function of air face velocity and temperature. Initially the process air temperature and humidity ratio have been kept constant and respectively equal to 30.0 °C ± 0.5 °C and 10.0 g kg^{-1} ± 0.1 g kg^{-1}. Then the air inlet temperature has been increased up to 67.2 °C. The revolution speed has been set at N = 10 rev h^{-1} (Appendix B).

4. Effectiveness correlations

As previously reported in Section 2, the effectiveness parameters η_ϕ and η_h described through Eqs. (1) and (2) are strongly dependent on all boundary conditions and cannot be considered constant over a wide range of operating conditions. Therefore two different independent correlations should be evaluated in order to predict properly the desiccant wheel effectiveness parameters for different inlet air states and revolution speed.

In the proposed correlations each effectiveness parameter is calculated as the product of five terms, referred to as α and β for η_ϕ and η_h respectively. Each term is assumed to be independent from the others and it takes into account the effect of one or more boundary conditions. In particular it has been evaluated that the effects of $T_{pro,in}$ and $T_{reg,in}$ can be grouped in one parameter (α_T and β_T) and, similarly, that the contribution of $X_{pro,in}$ and $X_{reg,in}$ can be coupled in a second one (α_X and β_X). Instead the contribution of $v_{reg,in}$, $v_{pro,in}$ and N is considered through an independent term (α_{vreg} and β_{vreg}, α_{vpro} and β_{vpro} and α_N and β_N respectively).

Many mathematical forms of both correlations have been investigated and evaluated, according to the theoretical deductions of Section 2.2. Each parameter α or β has been supposed to be linear, polynomial, exponential, logarithmic and power function of one or more air inlet states. All investigated correlations have been compared to effectiveness parameters calculated from experimental data, as reported in Section 3.3. The equations that minimize the root mean squared deviation have been selected.

Finally the proposed correlations to predict η_ϕ and η_h are reported respectively in Eqs. (8) and (9):

$$\begin{cases} \eta_\varphi = \alpha_{vreg}\alpha_{vpro}\alpha_T\alpha_X\alpha_N \\ \alpha_{vreg} = c_1 v_{reg,in}^2 + c_2 v_{reg,in} + c_3 \\ \alpha_{vpro} = c_4 v_{pro,in}^2 + c_5 v_{pro,in} + c_6 \\ \alpha_T = c_7 \ \ln(T_{reg,in} - T_{pro,in}) + c_8 \\ \alpha_X = c_9 X_{pro,in} + c_{10} X_{reg,in} + 1 \\ \alpha_N = c_{11} N + c_{12} \end{cases} \tag{8}$$

$$\begin{cases} \eta_h = \beta_{vreg}\beta_{vpro}\beta_T\beta_X\beta_N \\ \beta_{vreg} = k_1 \left(v_{reg,in}\right)^{k_2} \\ \beta_{vpro} = k_3 \left(v_{pro,in}\right)^{k4} \\ \beta_T = k_5 T_{reg,in} + k_6 T_{pro,in} + k_7 \\ \beta_X = k_8 X_{reg,in} + k_9 X_{pro,in} + 1 \\ \beta_N = k_{10} N + k_{11} \end{cases} \tag{9}$$

The adopted coefficients c_1–c_{12} and k_1–k_{11} are reported in Table 3. They have been calculated minimizing the root mean squared deviation between the correlation results and the actual values based on measurements.

In Eqs. (8) and (9), air temperature should be expressed in °C, the humidity ratio in kg kg^{-1} and the face velocity in m s^{-1} at inlet conditions of each stream. Note that the two proposed correlations are valid and should be used within the range of each boundary condition reported in Table 2.

Calculated and experimental relative humidity and enthalpy effectiveness indices are reported in Fig. 4. Relative error between predicted and measured values of η_ϕ is within ±5% in all the analyzed cases. On the other side, relative error of η_h is within ±5% and within ±10% respectively in 69.6% and 96.4% of the investigated working conditions.

In Figs. 5 and 6 it is investigated how such relative errors of effectiveness pair influence the estimation of the humidity ratio and temperature differences of the process air stream across the desiccant wheel, which are defined in the following way:

$$\Delta X_{pro} = X_{pro,in} - X_{pro,out} \tag{10}$$

$$\Delta T_{pro} = T_{pro,out} - T_{pro,in} \tag{11}$$

Table 2
Working conditions range of experimental tests performed to predict effectiveness parameters η_ϕ and η_h.

$T_{pro,in}$ (°C)	$X_{pro,in}$ (g kg^{-1})	$v_{pro,in}$ (m s^{-1})	$T_{reg,in}$ (°C)	$X_{reg,in}$ (g kg^{-1})	$v_{reg,in}$ (m s^{-1})	N (rev h^{-1})
17.6–33.8	9.1–17.4	1.75–2.85	44.4–78.6	8.4–16.3	1.64–2.53	4.9–25.6

Table 3
Coefficients adopted in the effectiveness pair correlations (Eqs. (8) and (9)).

c_1	c_2	c_3	c_4	c_5	c_6	c_7	c_8	c_9	c_{10}	c_{11}	c_{12}
−0.003286	0.020519	0.095525	0.008343	−0.04322	0.16501	1.1903	12.331	−4.519	0.80627	0.0030464	4.2846
k_1	k_2	k_3	k_4	k_5	k_6	k_7	k_8	k_9	k_{10}	k_{11}	
0.22113	0.23493	0.21763	−0.66335	0.0016778	−0.0056224	1.671	−44.505	27.728	0.13883	4.6438	

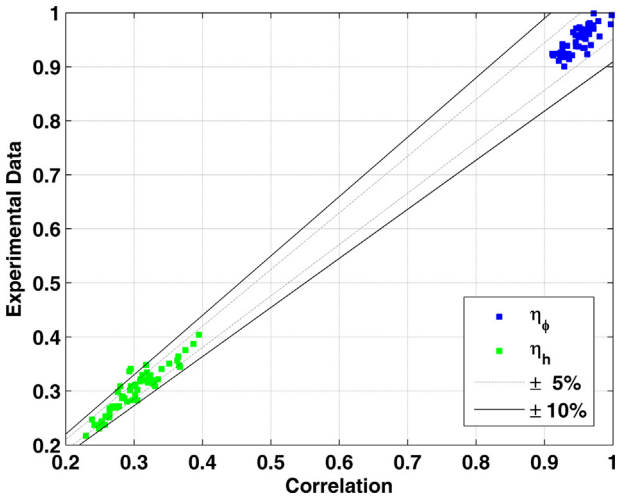

Fig. 4. Calculated and experimental η_ϕ and η_h.

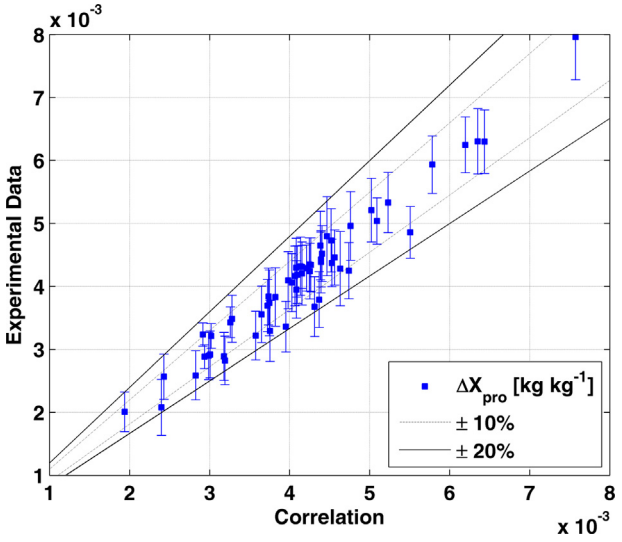

Fig. 5. Calculated and experimental ΔX_{pro} ($X_{pro,in} - X_{pro,out}$).

Experimental data are reported with calculated level of uncertainty. Relative error between predicted and measured values of ΔX_{pro} and ΔT_{pro} are within ±10% respectively in 82.1% and 98.2% of the analyzed cases. It should put in evidence that the predicted values of ΔX_{pro} are within the experimental uncertainty range in 89.3% of working conditions.

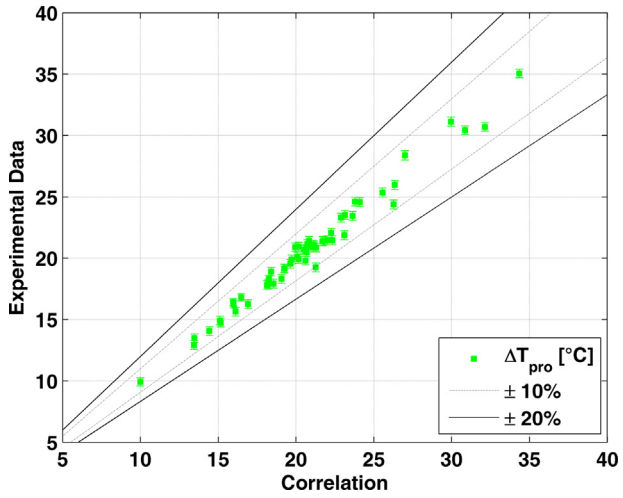

Fig. 6. Calculated and experimental ΔT_{pro} ($T_{pro,out} - T_{pro,in}$).

The temperature and humidity ratio root mean square error between calculated and measured data is evaluated through the following equations:

$$RMSE_T = \sqrt{\frac{\sum_{i=1}^{N_{test}} (T_{pro,out} - T_{pro,out,EXP})^2}{N_{test}}} \quad (12)$$

$$RMSE_X = \sqrt{\frac{\sum_{i=1}^{N_{test}} (X_{pro,out} - X_{pro,out,EXP})^2}{N_{test}}} \quad (13)$$

where the number of tests is N_{test} = 56. The resulting values of $RMSE_T$ and $RMSE_X$ are respectively 0.66 °C and 0.24 g kg^{-1}. In Table 4 these results are compared with the root mean square errors available in literature based on the constant effectiveness parameters approach. It is possible to state that the proposed correlations predict outlet process air conditions with good accuracy in relation to the constant effectiveness parameters investigated in literature. In addition it should be pointed out that in this work the revolution speed is not constant and air flow rates are considered both in balanced and unbalanced conditions.

Finally, in order to confirm the quality of the proposed correlations, in Figs. 7 and 8 the effect of the variation of each boundary condition on the effectiveness pair η_ϕ and η_h is evaluated through Eqs. (8) and 9. As expected from the considerations reported in Section 2.2, an increase in $v_{pro,in}$ leads to a decrease in η_ϕ and η_h, an increase in $T_{reg,in}$, $v_{reg,in}$ and N leads to an increase in η_ϕ and a variation of N causes a slightly variation of η_ϕ.

Table 4
$RMSE_T$ and $RMSE_X$: comparison between results of this works and data available in literature.

Reference	$RMSE_T$ (°C)	$RMSE_X$ (g kg^{-1})	$T_{pro,in}$ (°C)	$X_{pro,in}$ (g kg^{-1})	$V_{pro,in}$ (m^3 h^{-1})	$T_{reg,in}$ (°C)	$X_{reg,in}$ (g kg^{-1})	$V_{reg,in}$ (m^3 h^{-1})	N (rev h^{-1})	N_{test} (–)
This work	0.66	0.24	17.6–33.8	9.1–17.4	830–1350	44.4–78.6	8.4–16.3	780–1200	4.9–25.6	56
[4,25][a]	1.24	0.30	24–40	4–14	[c]	50–80	3–15	[c]	6	107
[27][a]	1.50	0.89	22.2–38.8	6.4–15.9	≈800[d]	49.8–68.6	6.4–15.9	≈800[d]	12	89
[27][b]	1.46	0.81	22.2–38.8	6.4–15.9	≈800[d]	49.8–68.6	6.4–15.9	≈800[d]	12	89
[44][a]	1.28	0.30	23.8–35.6	8.16–16.0	≈800[d]	51.0–70.2	8.16–16.0	≈800[d]	12	41

[a] Constant combined potential approach.
[b] Constant η_ϕ and η_h.
[c] Balanced flow conditions and flow rates equal to 600, 1000 and 1200 m^3 h^{-1}. Desiccant wheel diameter equal to 630 mm.
[d] Desiccant wheel diameter equal to 600 mm (60% of area crossed by process air stream).

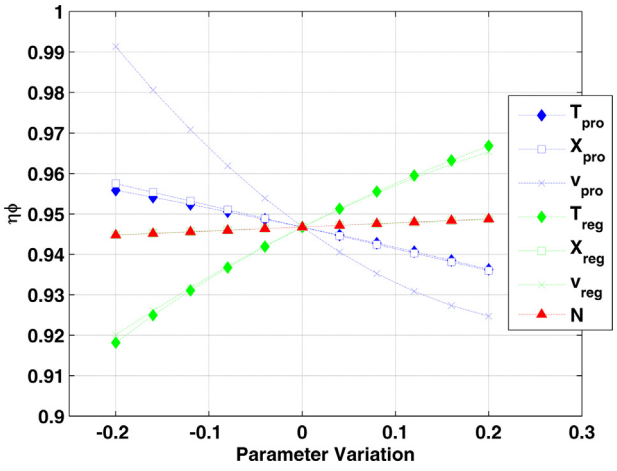

Fig. 7. Effects of boundary conditions on η_ϕ calculated through Eq. (8) (ref. condition: $T_{pro,in}$ = 25 °C, $X_{pro,in}$ = 12 g kg^{-1}, $v_{pro,in}$ = 2 m s^{-1}, $T_{reg,in}$ = 60 °C, $X_{reg,in}$ = 12 g kg^{-1}, $v_{reg,in}$ = 2 m s^{-1}, N = 15 rev h^{-1}).

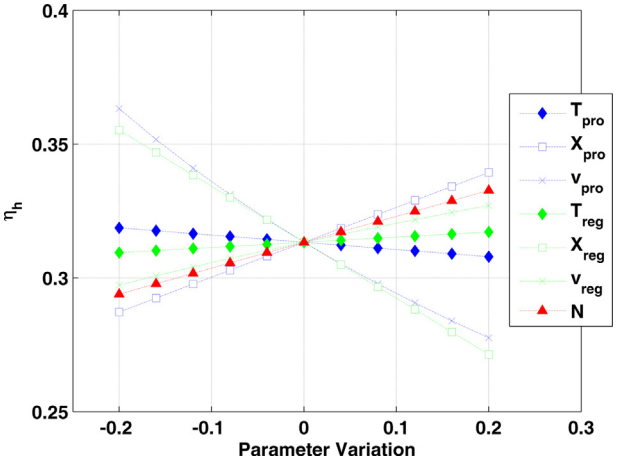

Fig. 8. Effects of boundary conditions on η_h calculated through Eq. (9) (ref. condition: $T_{pro,in}$ = 25 °C, $X_{pro,in}$ = 12 g kg^{-1}, $v_{pro,in}$ = 2 m s^{-1}, $T_{reg,in}$ = 60 °C, $X_{reg,in}$ = 12 g kg^{-1}, $v_{reg,in}$ = 2 m s^{-1}, N = 15 rev h^{-1}).

5. Pressure drop correlation

Total pressure drop across the desiccant wheel is evaluated in the following way:

$$\Delta P = x_1 \mu_a v_a + x_2 \rho_a v_a^2 \tag{14}$$

Table 5
Coefficients adopted in the pressure drop correlation (Eq. (14)).

x_1	x_2
3.77×10^6	6.5493

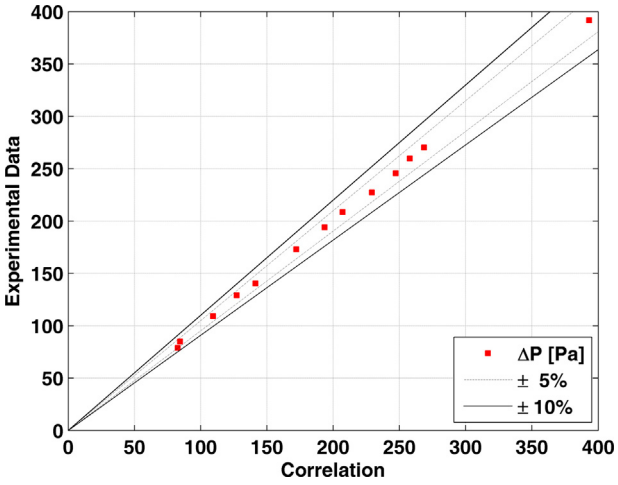

Fig. 9. Calculated and experimental pressure drop.

where the first and second term are respectively related to distributed and local pressure drop [45]. The dynamic viscosity μ_a has been evaluated in this form:

$$\mu_a = \frac{1.458 \times 10^{-6}(T_a + 273.15)^{1.5}}{T_a + 273.15 + 110.4} \tag{15}$$

Note that the measured pressure drop includes the effect of the cross section variation of the plenum which supplies the air flow to the device. In fact, the wheel face area has a semi circular geometry and the air plenum has a rectangular cross section. This effect has been taken into account in the proposed correlation through the term x_2.

In addition, referring to the wheel properties reported in Section 3.3, the distributed pressure drop calculated through the first term of Eq. (14) is in agreement with the one calculated with the friction factor $f = 11/Re$ and the wheel porosity $\sigma = 0.76$.

Air velocity is calculated at the wheel inlet section while air properties are evaluated at the mean condition between inlet and outlet states. The coefficients x_1 and x_2 used in Eq. (14) are reported in Table 5. In Fig. 9 calculated and experimental pressure drop are reported: the relative error is always within ±5%.

Table 6
Coefficients adopted in the effectiveness pair correlations to simulate an AQSOA zeolite desiccant wheel [46].

c_1	c_2	c_3	c_4	c_5	c_6	c_7	c_8	c_9	c_{10}	c_{11}	c_{12}
0	0	1	0	0	1	0.099038	0.586	−2.9435	0	0	1
k_1	k_2	k_3	k_4	k_5	k_6	k_7	k_8	k_9	k_{10}	k_{11}	
1	0	1	0	0.00058696	−0.00077447	0.16886	−3.9466	0	0	1	

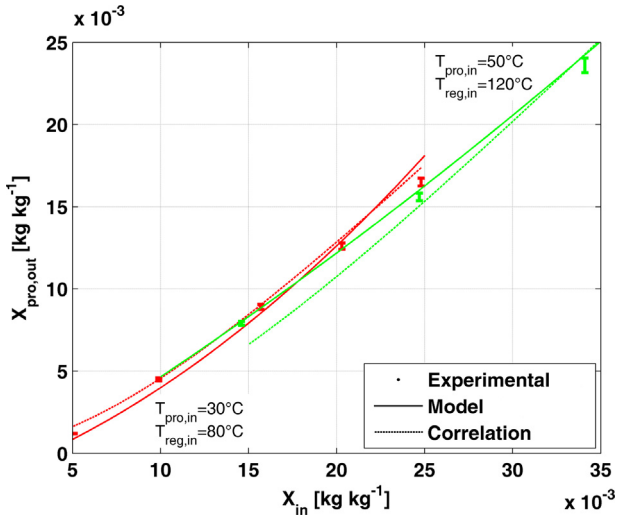

Fig. 10. Outlet process air humidity ratio (ref. condition: v_{in} = 2 m s^{-1}, N = 20 rev h^{-1}, $X_{pro,in} = X_{reg,in}$ [46]).

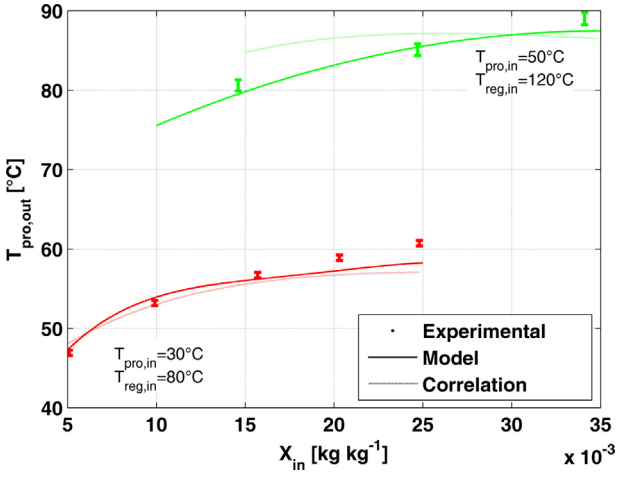

Fig. 11. Outlet process air temperature (ref. condition: v_{in} = 2 m s^{-1}, N = 20 rev h^{-1}, $X_{pro,in} = X_{reg,in}$ [46]).

6. Application of the proposed effectiveness correlations to a different desiccant wheel

In order to confirm the validity of the proposed formulation, the effectiveness correlations are adopted for an AQSOA zeolite desiccant wheel, whose experimental data are available in literature [46]. In fact, as clearly shown in previous works [12,14,47,48], desiccant wheel performance strongly depends on its physical and chemical properties. If a model based on heat and mass transfer equations is used to evaluate component performance, desiccant wheel specific properties (such as channel geometry, adsorption isotherm, specific heat, thermal conductivity, etc.) should be adopted.

The aim of this section is to show how the proposed correlations, which indirectly take into account the characteristics of the investigated component, can be adopted to fit data of a generic desiccant wheel. It is highlighted that good results are obtained also in case of different sorption materials and physical and chemical properties.

The analyzed desiccant wheel is made of AQSOA zeolite and channels have a sinusoidal cross sectional area with height equal to 1.5 mm and base equal to 3.4 mm. The wheel diameter and thickness are respectively equal to 0.32 m and 0.2 m. Further components data are available in literature [46].

At a first stage the correlations (Eqs. (8) and (9)) are calibrated through the available experimental data, summarized in Appendix C. Note that, according to ASHRAE [49],if $p_{vsat} > p_{tot}$ the relative humidity is not defined. Therefore in this condition the term ϕ of Eq. (1) is simply defined as $\phi = p_v/p_{vsat}$. The resulting coefficients are reported in Table 6. It is put in evidence that:

- Experimental data are available only at constant revolution speed and face velocity and at equal inlet humidity ratio. Quite obviously the Eqs. (8) and (9), coupled with coefficients of Table 6, can be used only according to the experimental data set used to fit the correlations, namely N = 20 rev h^{-1}, $v_{pro,in} = v_{reg,in} = v_{in}$ = 2 m s^{-1}, $X_{pro,in} = X_{reg,in} = X_{in}$ = 5–35 g kg^{-1}, $T_{pro,in}$ = 30–50 °C and $T_{reg,in}$ = 60–120 °C.
- Therefore correlations must be independent on N, $v_{pro,in}$, and $v_{reg,in}$ and may depend only on X_{in} instead of $X_{pro,in}$ and $X_{reg,in}$.
- As a consequence, according to Table 6, the terms α_N, α_{vreg}, α_{vpro}, β_N, β_{vreg} and β_{vpro} are set equal to 1 and terms α_X and β_X are modified in order to take into account that $X_{pro,in}$ and $X_{reg,in}$ vary together and that no information about the independent variation of each inlet humidity ratio is available. Therefore, being $X_{pro,in} = X_{reg,in} = X_{in}$, it becomes $\alpha_X = C_9 X_{in} + 1$ and $\beta_X = k_8 X_{in} + 1$.

In Figs. 10 and 11 correlations results are compared with experimental data and with results of a detailed gas solid side resistance model [46] in different working conditions. It is possible to state that correlations properly predict outlet conditions, in particular at low process and regeneration air temperature.

7. Conclusions

In this work the use of effectiveness parameters to determine desiccant wheel performance is investigated. The adopted effectiveness pair η_ϕ and η_h is based on relative humidity and enthalpy differences. The performance of a commercial desiccant wheel is evaluated on a specific test rig in a wide range of operating conditions. Accurate correlations based on experimental data to predict desiccant wheel performance and pressure drop are proposed. The obtained correlations predict properly the actual desiccant wheel effectiveness and, therefore, humidity ratio drop and temperature rise of process air stream across the desiccant wheel. It is shown that the relative error between predicted and measured values of ΔX_{pro} and ΔT_{pro} is within ±10% respectively in 82.1% and 98.2% of the analyzed cases and the root mean square errors $RMSE_T$ and $RMSE_X$ are respectively 0.66 °C and 0.24 g kg^{-1}. The relative error between calculated and measured values of pressure drop is always within ±5%. Finally it is shown how the correlations can be used

Table A.1
Experimental tests performed to evaluate effectiveness pair correlations.

Test (–)	$T_{pro,in}$ (°C)	$X_{pro,in}$ (g kg^{-1})	$v_{pro,in}$ (m s^{-1})	$T_{reg,in}$ (°C)	$X_{reg,in}$ (g kg^{-1})	$v_{reg,in}$ (m s^{-1})	N (rev h^{-1})	$T_{pro,out}$ (°C)	$X_{pro,out}$ (g kg^{-1})
1	30.6	11.7	2.14	63.6	11.9	2.41	5.9	49.0	7.5
2	29.5	11.7	2.12	63.9	12.2	2.41	8.5	49.5	7.4
3	30.1	11.7	2.10	55.1	12.0	2.34	10.5	45.0	8.8
4	30.4	11.0	2.13	66.1	12.2	2.45	10.5	51.2	6.9
5	29.4	11.5	2.14	65.2	11.8	2.44	10.5	50.2	7.7
6	30.1	11.1	2.53	55.6	12.1	2.62	10.5	44.2	8.2
7	31.0	12.3	2.09	64.2	12.9	2.36	12.5	51.9	8.0
8	30.3	11.7	2.09	64.4	12.3	2.43	12.5	50.8	7.5
9	30.4	11.1	2.12	65.0	12.8	2.45	12.5	50.6	7.3
10	29.9	10.9	1.81	64.4	11.7	2.03	15.5	51.3	7.1
11	18.9	9.3	2.07	70.6	11.0	2.39	15.5	49.3	4.3
12	29.9	11.8	2.09	55.5	11.9	2.35	15.5	45.5	9.0
13	19.0	9.7	2.10	44.4	9.4	2.35	15.5	35.4	6.5
14	17.6	9.3	2.10	44.5	9.5	2.30	15.5	34.5	6.1
15	30.1	17.4	2.10	57.1	11.0	2.32	15.5	50.0	11.2
16	31.1	9.1	2.10	71.3	10.6	2.38	15.5	54.7	5.4
17	19.8	9.9	2.10	72.9	11.2	2.43	15.5	50.5	5.0
18	31.1	10.6	2.10	75.3	11.9	2.39	15.5	55.5	6.3
19	30.0	11.0	2.11	52.4	11.9	2.28	15.5	43.5	8.4
20	33.8	11.0	2.11	56.2	12.0	2.34	15.5	46.7	8.9
21	30.6	17.2	2.12	74.7	10.7	2.34	15.5	61.7	9.2
22	30.1	11.8	2.13	65.3	11.7	2.44	15.5	51.5	8.1
23	29.7	11.6	2.13	69.4	12.3	2.38	15.5	54.3	6.9
24	21.1	10.9	2.14	51.4	12.1	2.34	15.5	39.4	7.5
25	28.1	12.3	2.14	61.7	13.1	2.34	15.5	48.8	8.9
26	30.6	11.1	2.14	66.2	10.4	2.41	15.5	52.0	6.7
27	29.9	12.5	2.49	68.7	11.7	2.70	15.5	54.5	7.3
28	27.0	15.2	2.50	58.3	16.1	2.81	15.5	46.2	10.9
29	29.9	11.3	2.52	55.6	12.1	2.62	15.5	44.6	8.4
30	30.0	10.9	2.54	66.3	11.7	2.78	15.5	51.0	6.9
31	29.7	11.6	2.10	64.6	12.1	2.44	25.6	51.5	8.3
32	29.5	12.2	2.13	69.7	12.7	2.38	25.6	55.4	7.6
33	29.6	11.8	2.14	55.4	12.2	2.35	25.6	45.8	9.2
34	30.1	12.3	2.50	69.2	11.4	2.71	25.6	55.4	7.3
35	29.5	11.5	2.15	65.5	11.5	2.85	4.9	48.8	7.2
36	31.3	14.4	2.09	64.1	8.4	2.13	5.4	52.7	8.1
37	31.7	11.8	2.10	65.3	12.5	1.86	5.9	49.6	7.7
38	29.2	11.2	2.13	64.9	11.4	2.85	5.9	50.1	6.7
39	29.4	11.3	2.12	64.3	11.8	2.85	6.9	50.4	6.9
40	29.6	11.6	2.14	63.5	12.1	2.41	6.9	49.1	7.3
41	30.1	11.4	2.11	63.4	12.5	1.90	8.5	47.9	7.7
42	29.4	11.5	2.11	64.3	11.9	2.85	8.5	50.5	7.0
43	31.4	14.4	2.10	64.4	8.4	2.13	10.5	53.5	8.1
44	30.5	11.4	2.11	64.6	12.1	2.85	10.5	51.6	7.1
45	29.6	12.7	2.57	68.3	11.9	2.70	10.5	52.9	7.4
46	31.2	11.8	2.09	64.4	12.6	1.75	12.5	49.1	8.2
47	30.8	11.5	2.15	64.8	12.2	2.85	12.5	52.2	7.3
48	30.0	11.0	1.77	64.5	11.6	2.81	15.5	53.4	6.8
49	27.1	11.3	2.08	63.3	16.3	2.49	15.5	48.0	7.8
50	31.8	9.4	2.09	78.6	10.8	2.29	15.5	60.1	4.6
51	29.4	9.3	2.10	45.4	9.1	2.34	15.5	39.3	7.3
52	19.8	9.6	2.12	77.8	10.6	2.29	15.5	54.8	3.7
53	18.2	9.3	2.14	45.7	9.1	1.81	15.5	34.4	6.4
54	28.6	12.2	2.26	58.6	13.0	2.66	15.5	47.5	9.0
55	25.9	15.2	2.31	57.5	16.0	2.34	15.5	45.1	10.9
56	26.8	15.1	2.53	61.0	16.1	2.61	15.5	46.6	10.7

to fit available experimental data of a generic desiccant wheel, in order to predict effectiveness of the device regardless its sorption materials and geometry.

The proposed correlations are able to predict the performance of the desiccant wheel properly. Due to their simple formulation, they are particularly suitable for energy simulation tools for building – HVAC systems.

Acknowledgment

Funding for this work from Cassa Conguaglio Sistema Elettrico (CCSE) under agreement no. 6562 is acknowledged (project STAR — Sidera Trigenerazione Alto Rendimento).

Appendix A.

In Table A.1 tests results used to evaluate effectiveness pair correlations are reported. In tests 1–34 the mass air flows (kg s^{-1}) are almost balanced while in tests 35–56 regeneration and process air flows are unbalanced. Each set of tests is ranked by increasing values of N, v_{pro} and T_{reg}.

Appendix B.

Table B.1

Table B.1
Experimental tests performed to evaluate pressure drop correlation.

Test (–)	$v_{pro,in}$ (m s^{-1})	T_a (°C)	X_a (g kg^{-1})	ΔP (Pa)
1	1.08	29.6	9.8	84.9
2	1.56	29.6	10.0	129.1
3	2.23	29.8	10.1	194.0
4	2.83	29.8	10.1	259.7
5	2.92	29.7	10.2	270.1
6	3.95	29.7	10.0	391.7
7	0.99	67.2	10.0	78.7
8	1.29	65.3	10.0	109.2
9	1.63	63.8	10.1	140.4
10	1.94	63.2	10.2	172.9
11	2.27	63.3	9.9	208.6
12	2.49	58.0	10.0	227.3
13	2.63	67.1	10.1	245.7

Table C.1
Experimental tests of an AQSOA zeolite desiccant wheel [46] ($v_{pro,in} = v_{reg,in} = 2$ m s^{-1}).

Test (–)	$T_{pro,in}$ (°C)	X_{in} (g kg^{-1})	$T_{reg,in}$ (°C)	N (rev h^{-1})	$T_{pro,out}$ (°C)	$X_{pro,out}$ (g kg^{-1})
1	30	5.5	60	20	42.1	2.9
2	30	10.0	60	20	45.2	6.4
3	30	15.4	60	20	46.7	11.2
4	30	24.3	60	20	43.9	19.6
5	30	5.1	80	20	46.9	1.2
6	30	9.9	80	20	53.2	4.5
7	30	15.7	80	20	56.7	8.9
8	30	20.3	80	20	58.9	12.6
9	30	24.8	80	20	60.7	16.5
10	50	15.7	100	20	72.8	10.2
11	50	24.8	100	20	76.2	17.7
12	50	34.7	100	20	78.0	26.8
13	50	14.6	120	20	80.6	7.9
14	50	24.7	120	20	85.1	15.6
15	50	34.1	120	20	89.0	23.6

Appendix C.

Table C.1

References

[1] D. Kadoma, R.Z. Wang, Z.Z. Xia, Desiccant cooling air conditioning: a review, Renew. Sustain. Energy Rev. 10 (2) (2006) 55–77.
[2] T.S. Ge, Y.J. Dai, R.Z. Wang, Review on solar powered rotary desiccant wheel cooling system, Renew. Sustain. Energy Rev. 39 (2014) 476–497.
[3] W. Gao, W. Worek, V. Konduru, K. Adensin, Numerical study on performance of a desiccant cooling system with indirect evaporative cooler, Energy Build. 86 (2015) 16–24.
[4] G. Panaras, E. Mathioulakis, V. Belessiotis, N. Kyriakis, Theoretical and experimental investigation of the performance of a desiccant air-conditioning system, Renew. Energy 35 (7) (2010) 1368–1375.
[5] M. O'Kelly, M.E. Walter, J.R. Rowland, Simulated hygrothermal performance of a desiccant-assisted hybrid air/water conditioning system in a mixed humid climate under dynamic load, Energy Build. 86 (2015) 45–57.
[6] G. Angrisani, F. Minichiello, C. Roselli, M. Sasso, Desiccant HVAC system driven by a micro-CHP: experimental analysis, Energy Build. 42 (11) (2010) 2028–2035.
[7] W. Liu, Z. Lian, R. Radermacher, Y. Yao, Energy consumption analysis on a dedicated outdoor air system with rotary desiccant wheel, Energy 32 (9) (2007) 1749–1760.
[8] S. De Antonellis, C.M. Joppolo, L. Molinaroli, A. Pasini, Simulation and energy efficiency analysis of desiccant wheel systems for drying processes, Energy 37 (1) (2012) 336–345.
[9] Y.J. Dai, R.Z. Wang, Y.X. Xu, Study of a solar powered solid adsorption – desiccant cooling system used for grain storage, Renew. Energy 25 (3) (2002) 417–430.
[10] W.C. Wang, R.K. Calay, Y.K. Chen, Experimental study of an energy efficient hybrid system for surface drying, Appl. Therm. Eng. 31 (4) (2011) 425–431.
[11] S. De Antonellis, C.M. Joppolo, L. Molinaroli, Simulation, performance analysis and optimization of desiccant wheels, Energy Build. 42 (9) (2010) 1386–1393.
[12] S.D. White, M. Goldsworthy, R. Reece, T. Spillmann, A. Gorur, D.Y. Lee, Characterization of desiccant wheels with alternative materials at low regeneration temperatures, Int. J. Refrig. 34 (8) (2011) 1786–1791.
[13] T.S. Ge, Y. Li, R.Z. Wang, Y.J. Dai, A review of the mathematical models for predicting rotary desiccant wheel, Renew. Sustain. Energy Rev. 12 (2008) 1485–1528.
[14] U. Eicker, U. Schürger, M. Köhler, T. Ge, Y. Dai, H. Li, R.Z. Wang, Experimental investigations on desiccant wheels, Appl. Therm. Eng. 42 (2012) 71–80.
[15] N. Enteria, H. Yoshino, A. Satake, A. Mochida, R. Takaki, R. Yoshie, T. Mitamura, S. Baba, Experimental heat and mass transfer of the separated and coupled rotating desiccant wheel and heat wheel, Exp. Therm. Fluid Sci. 34 (5) (2010) 603–615.
[16] A.M. Baniyounes, M.G. Rasul, M.M.K. Khan, Experimental assessment of a solar desiccant cooling system for an institutional building in subtropical Queensland, Australia, Energy Build. 62 (2013) 78–86.
[17] Y. Sheng, Y. Zhang, Y. Sun, L. Fang, J. Nie, L. Ma, Experimental analysis and regression prediction of desiccant wheel behavior in high temperature heat pump and desiccant wheel air-conditioning system, Energy Build. 80 (2014) 358–365.
[18] R. Tu, X.H. Liu, Y. Jiang, Performance analysis of a two-stage desiccant cooling system, Appl. Energy 113 (2014) 1562–1574.
[19] X. Zheng, T.S. Ge, R.Z. Wang, Recent progress on desiccant materials for solid desiccant cooling systems, Energy 74 (2014) 280–294.
[20] L.Z. Zhang, Energy performance of independent air dehumidification systems with energy recovery measures, Energy 31 (2006) 1228–1242.
[21] P. Bourdoukan, E. Wurtz, P. Joubert, Comparison between the conventional and recirculation modes in desiccant cooling cycles and deriving critical efficiencies components, Energy 35 (2010) 1057–1067.
[22] Z. Hatami, M.H. Saidi, M. Mohammadian, C. Aghanajafi, Optimization of solar collector surface in solar desiccant wheel cycle, Energy Build. 45 (2013) 197–201.
[23] M. Beccali, F. Butera, R. Guanella, R.S. Adhikari, Simplified models for the performance evaluation of desiccant wheel dehumidification, Int. J. Energy Res. 27 (1) (2003) 17–29.
[24] M. Beccali, R.S. Adhikari, F. Butera, V. Franzitta, Update on desiccant wheel model, Int. J. Energy Res. 28 (12) (2014) 1043–1049.
[25] G. Panaras, E. Mathioulakis, V. Belessiotis, N. Kyriakis, Experimental validation of a simplified approach for a desiccant wheel model, Energy Build. 42 (10) (2010) 1719–1725.
[26] J.J. Jurinak, Open Cycle Desiccant Cooling – Component Models and System Simulations (Ph.D. thesis), University of Wisconsin, Madison, 1982.
[27] C.R. Ruivo, G. Angrisani, The effectiveness method to predict the behaviour of a desiccant wheel: an attempt of experimental validation, Appl. Therm. Eng. 71 (2) (2014) 643–651.
[28] A.E. Kabeel, Solar powered air conditioning system using rotary honeycomb desiccant wheel, Renew. Energy 32 (11) (2007) 1842–1857.
[29] J.L. Niu, L.Z. Zhang, Effects of wall thickness on the heat and moisture transfers in desiccant wheels for air dehumidification and enthalpy recovery, Int. Commun. Heat Mass Transf. 29 (2) (2002) 255–268.
[30] M. Ali Mandegari, H. Pahlavanzadeh, Introduction of a new definition for effectiveness of desiccant wheels, Energy 34 (6) (2009) 797–803.
[31] C.R. Ruivo, J.J. Costa, A.R. Figueiredo, A. Kodama, Effectiveness parameters for the prediction of the global performance of desiccant wheels – an assessment based on experimental data, Renew. Energy 38 (1) (2012) 181–187.
[32] C.R. Ruivo, A. Carrillo-Andrés, J.J. Costa, F. Domínguez-Muñoz, A new approach to the effectiveness method for the simulation of desiccant wheels with variable inlet states and airflows rates, Appl. Therm. Eng. 58 (1) (2013) 670–678.
[33] C.R. Ruivo, A. Carrillo-Andrés, J.J. Costa, F. Domínguez-Muñoz, Exponential correlations to predict the dependence of effectiveness parameters of a desiccant wheel on the airflow rates and on the rotation speed, Appl. Therm. Eng. 51 (1) (2013) 442–450.
[34] C.R. Ruivo, A. Carrillo-Andrés, J.J. Costa, F. Domínguez-Muñoz, Interpolation procedures for the effectiveness method to account for the influence of the inlet airflow states on the desiccant wheels performance, Energy Build. 55 (2012) 380–388.
[35] C.R. Ruivo, M. Goldsworthy, M. Intini, Interpolation methods to predict the influence of inlet airflow states on desiccant wheel performance at low regeneration temperature, Energy 68 (2014) 765–772.
[36] C.R. Ruivo, G. Angrisani, M. Minichiello, Influence of the rotation speed on the effectiveness parameters of a desiccant wheel: an assessment using experimental data and manufacturer software, Renew. Energy 76 (2015) 484–493.
[37] M. Intini, S. De Antonellis, C.M. Joppolo, The effect of inlet velocity and unbalanced flows on optimal working conditions of silica gel desiccant wheels, Energy Procedia 48 (2014) 858–864.
[38] T. Kuma, T. Hirose, M. Goto, A. Kodama, Thermally regenerative monolithic rotor dehumidifier for adsorption cooling system, J. Sol. Energy Eng. 120 (1) (1998) 45–50.
[39] DIN EN ISO 5167-2 Standards, Measurement of Fluid Flow by Means of Pressure Differential Devices Inserted in Circular Cross-section Conduits Running Full—Part 2: Orifice Plates (ISO 5167-2:2003).
[40] ISO IEC Guide 98-3, Uncertainty of Measurement—Part 3: Guide to Expression of Uncertainty in Measurement, International Organization for Standardization, ISO IEC Guide 98-3, Geneva, Switzerland, 2008.

[41] R.J. Moffat, Describing the uncertainties in experimental results, Exp. Therm. Fluid Sci. 1 (1) (1988) 3–17.
[42] J.L. Niu, L.Z. Zhang, Heat transfer and friction coefficients in corrugated ducts confined by sinusoidal and arc curves, Int. J. Heat Mass Transf. 45 (3) (2002) 571–578.
[43] R.S.W. Sing, D.H. Everett, R.A.W. Haul, L. Moscou, R.A. Pierotti, J. Rouquerol, T. Siemieniewska, Reporting physisorption data for gas/solid systems with special reference to the determination of surface area and porosity (Recommendations 1984), Pure Appl. Chem. 57 (4) (1985) 603–619.
[44] G. Angrisani, C. Roselli, M. Sasso, Experimental validation of constant efficiency models for the subsystems of an unconventional desiccant-based Air Handling Unit and investigation of its performance, Appl. Therm. Eng. (33–34) (2012) 100–108.
[45] S. De Antonellis, M. Intini, C.M. Joppolo, F. Pedranzini, Experimental analysis and practical effectiveness correlations of enthalpy wheels, Energy Build. 84 (2014) 316–323.
[46] M. Intini, M. Goldsworthy, S. White, C.M. Joppolo, Experimental analysis and numerical modelling of an AQSOA zeolite desiccant wheel, Appl. Therm. Eng. 80 (2015) 20–30.
[47] L.Z. Zhang, J.L. Niu, Performance comparisons of desiccant wheels for air dehumidification and enthalpy recovery, Appl. Therm. Eng. 22 (2002) 1347–1367.
[48] L.Z. Zhang, H.X. Fu, Q.R. Yang, J.C. Xu, Performance comparisons of honeycomb-type adsorbent beds (wheels) for air dehumidification with various desiccant wall materials, Energy 65 (2014) 430–440.
[49] Psychrometrics: Theory and Practice, ASHRAE, Atlanta, 1996.